CHAPTER 2

Biological validation of a boronic acid-based inhibitor of autotaxin reveals rapid turnover of LPA in the circulation

Harald M.H.G. Albers, Anping Dong, Laurens A. van Meeteren, David A. Egan, Manjula Sunkara, Erica W. van Tilburg, Karianne Schuurman, Olaf van Tellingen, Andrew J. Morris, Susan S. Smyth, Wouter H. Moolenaar and Huib Ovaa, *Proceedings of the National Academy of Sciences of the United States of America* **2010**, *107*, 7257-7262.

Abstract. Autotaxin (ATX or ENPP2) is a secreted ecto-nucleotide pyrophosphatase/phosphodiesterase (ENPP) that functions as a lysophospholipase D to produce the lipid mediator lysophosphatidic acid (LPA), a mitogen, chemoattractant and survival factor for many cell types. The ATX-LPA axis has been implicated in angiogenesis, chronic inflammation and tumor progression, making this system an attractive target for therapy. However, potent and selective non-lipid inhibitors of ATX were not available at the beginning of this study. By screening a chemical library, thiazolidine-2,4-diones have been identified that selectively inhibit ATX-mediated LPA production both *in vitro* and *in vivo*. Inhibitor potency was a 100-fold increased (IC_{50} ~30 nM, HA130) after the incorporation of a boronic acid moiety, designed to target the active site threonine (T210) in ATX. Intravenous injection of this inhibitor into mice resulted in a rapid decrease in plasma LPA levels, indicating that turnover of LPA in the circulation is much more dynamic than previously appreciated. Thus, boronic acid-based small molecules hold promise as candidate drugs to target ATX.

2.1 Introduction

Autotaxin (ATX or ENPP2) is a secreted ecto-nucleotide pyrophosphatase/ phosphodiesterase (ENPP) originally isolated as an autocrine motility factor from melanoma cells.[1] ATX, a ~120 kDa glycoprotein, is unique amongst the ENPPs in that it functions as a lysophospholipase D (lysoPLD) that converts extracellular lysophosphatidylcholine (LPC) into the lipid mediator lysophosphatidic acid (LPA).[2-5] LPA acts on specific G protein-coupled receptors and thereby stimulates the migration, proliferation and survival of many cell types (Figure 1).[6,7] ATX is produced by various tissues and is the major LPA-producing enzyme in the circulation. Newly produced LPA is subject to degradation by membrane-bound lipid phosphate phosphatases (LPPs).[8,9] However, little is known about the dynamic regulation of steady-state LPA levels *in vivo*.

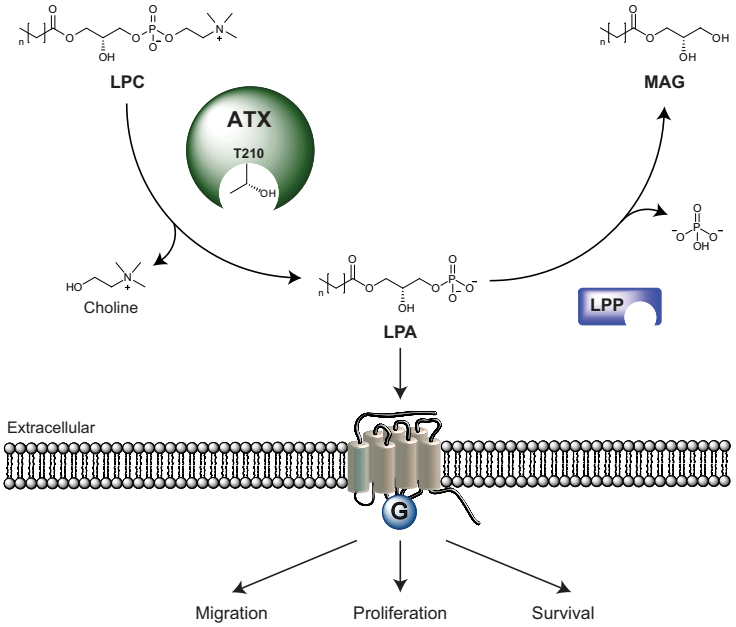

Figure 1: The ATX-LPA receptor signaling axis. Secreted ATX hydrolyzes extracellular LPC into LPA, a reaction catalyzed by active site residue T210. LPA signals through multiple G protein-coupled receptors to stimulate the proliferation, migration and survival of many cell types. LPA is degraded to monoacylglycerol (MAG) by lipid phosphate phosphatases (LPPs), which are membrane-bound ecto-enzymes.

ATX is essential for vascular development[10,11] and is found overexpressed in various human cancers.[12] Forced overexpression of ATX or individual LPA receptors promotes tumor progression in mouse models,[13-16] while LPA receptor deficiency protects from colon carcinogenesis.[17] In addition, to its role in cancer, ATX-LPA signaling has been implicated in lymphocyte homing and (chronic) inflammation,[18] fibrotic diseases[19,20] and thrombosis.[21] Therefore, the ATX-LPA axis qualifies as an attractive target for therapies.

Potent and selective ATX inhibitors are now needed as a starting point for the development of targeted anti-ATX/LPA therapy. Direct targeting of LPA receptors seems to be a less attractive strategy, since LPA acts on multiple receptors that show overlapping activities.[5,7] Since the initial finding that ATX is subject to product inhibition by LPA and sphingosine 1-phosphate (S1P),[22] various synthetic phosphate and phosphonate lipids have been explored as ATX inhibitors.[23-26] However, such lipid inhibitors have the inherent danger of inadvertently activating downstream LPA/S1P receptors, thereby inducing the opposite of the intended effect. Furthermore, lipids offer relatively few avenues for chemical diversification and usually have poor pharmacokinetic properties. Non-lipid inhibitors of ATX have recently been identified, but their potencies are low.[27]

In this study we screened small molecule libraries to search for novel ATX inhibitors. We identified thiazolidine-2,4-dione compounds that selectively inhibit ATX activity and are readily amenable to further chemical diversification. We have optimized these molecules by adopting an active site-targeted strategy that has proved successful for the development of the boronic acid-based proteasome inhibitor bortezomib,[28] which is in clinical use.[29] We show that a boronic acid-based inhibitor potently inhibits ATX both *in vitro* and *in vivo*. When administered to mice, our inhibitor (HA130) induces a remarkably rapid fall in plasma LPA levels, indicating that the turnover of circulating LPA is much more dynamic than previously appreciated. We conclude that boronic acid-based inhibitors hold promise as candidate drugs to target the ATX-LPA axis *in vivo*.

2.2 Discovery of small molecule inhibitors of ATX

The hydrolytic activity of ATX originates from a single catalytic site at threonine 210 (T210) in the central phosphodiester domain (Figure 1).[2] To discover novel ATX inhibitors, we screened a collection of ~40,000 drug-like small molecules using the hydrolysis of bis-*para*-nitrophenyl phosphate (bis-pNPP) by ATX as a readout. Among the most potent hits, we selected a

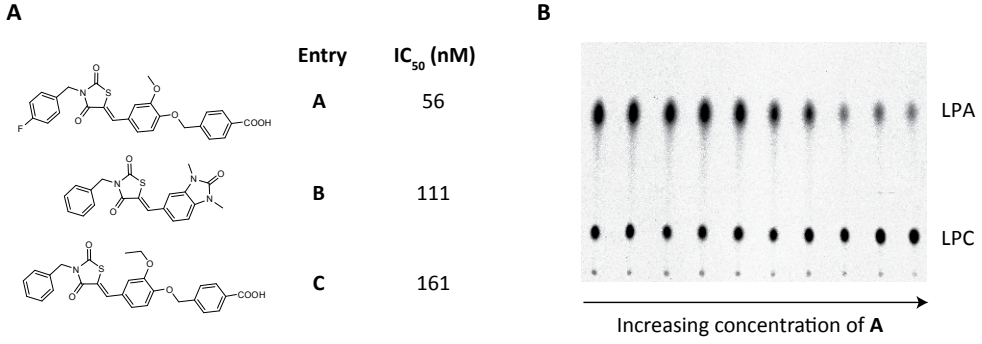

Figure 2: ATX inhibitors discovered by high-throughput screening and validation of compound **A**. (A) IC_{50} values based on bis-pNPP (1 mM) hydrolysis. (B) TLC analysis of ^{14}C-LPC to ^{14}C-LPA conversion at different concentrations of **A** (range: 0-30 μM).

thiazolidine-2,4-dione series for optimization since the thiazolidine-2,4-dione core is readily amenable to chemical diversification (Figure 2A). Inhibitor **A** showed an IC_{50} value of 56 nM using 1 mM bis-pNPP as substrate. For validation of **A**, we measured the inhibition of the ATX-catalyzed release of choline from LPC. We established that recombinant ATX has a K_m value for LPC of 94 µM (Supporting Figure S1). Compound **A** inhibited ATX with an IC_{50} value of 2.5 µM using 40 µM LPC as a substrate (Figure 3A). However, it should be noted that **A** has a 35% residual ATX activity (Figure 3B). Inhibition of ATX-mediated LPA production was confirmed by measuring the conversion of ^{14}C-LPC to ^{14}C-LPA using thin-layer chromatography (Figure 2B).

2.3 Boronic acid-based optimization

Having identified compound **A** as a novel ATX inhibitor, we set out to improve its potency. We engineered a synthetic route (see Chapter 3), which allowed the synthesis and isolation of more than 100 derivatives of **A** in a short time frame.

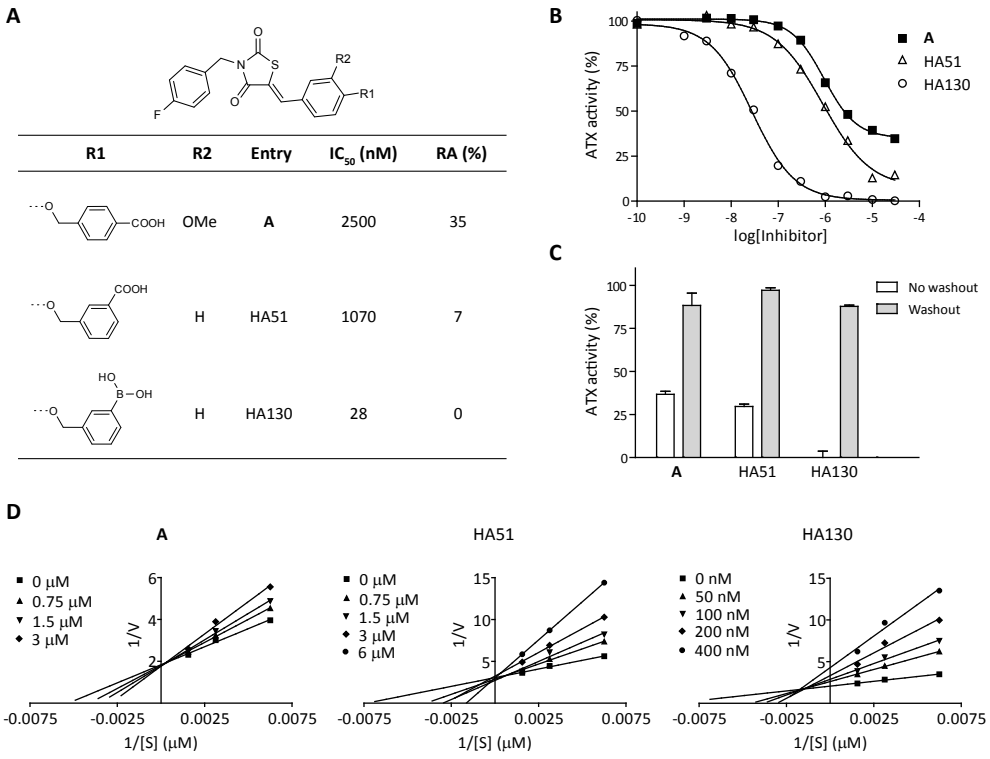

Figure 3: Analysis of ATX inhibition by compounds **A**, HA51 and boronic acid HA130, as measured by choline release from LPC (40 µM). (A) IC_{50} values and residual ATX activity (RA) for the three inhibitors tested. (B) Dose-inhibition curves for the inhibitors shown in (A). (C) Washout experiments showing that ATX inhibition is reversible. (D) Lineweaver-Burk plot analysis of ATX inhibition, showing competitive inhibition by **A** and HA51 and mixed-type inhibition by HA130.

All derivatives were tested in the ATX-mediated choline release assay. Figure 3A shows the IC_{50} values of the three most important molecules in the optimization process. Omitting the methoxy group and replacing the carboxylic acid to the *meta* position (HA51) resulted in a 2.5-fold increase in potency, concomitant with a significant drop in residual ATX activity, from 35 to 7% (Figure 3A and B). Lineweaver-Burk analysis revealed that **A** and HA51 act as competitive inhibitors (Figure 3D), suggesting that they bind at or close to the catalytic threonine residue (T210).

We next sought to target active site residue T210. We reasoned that the acid moiety of **A** and HA51 may bind to the phosphate ester acceptor site in ATX and that the T210 oxygen nucleophile could be targeted by a boronic acid moiety. Boronic acid is known for its high affinity for hard oxygen nucleophiles over soft nucleophiles, such as sulfur, which is found in many phosphate ester hydrolytic enzymes. This approach has an important precedent in the proteasome inhibitor and anti-cancer drug bortezomib (Velcade), which is a peptidyl boronic acid that targets the threonine oxygen nucleophile in the proteasome active site through its boronic acid moiety.[28,30] We adopted a similar approach to target the T210 oxygen nucleophile in ATX. This improves selectivity over phosphate ester hydrolyzing enzymes that depend on a sulfur (cysteine) nucleophile.

Replacing the carboxylic acid in HA51 by a boronic acid yielded compound HA130. This resulted in a ~100-fold increase in potency compared to screening hit **A** (IC_{50} = 28 nM) (Figure 3A). Furthermore, HA130 abolished the residual ATX activity observed with inhibitors **A** and HA51. Kinetic analysis revealed that HA130 is a mixed-type inhibitor, producing a reduction in V_{max} and an increase in K_m (Figure 3D). Thus, inhibition of ATX by HA130 results from a combination of a decreased turnover number and decreased affinity for its substrate. Washout of HA130 and the other inhibitors fully restored ATX activity, indicative of reversible inhibition (Figure 3C).

2.4 Selective inhibition of ATX

Since boronic acids can target the proteasome active site, we examined whether HA130 may affect proteasome activity. HA130 did not affect the chymotryptic, caspase and tryptic activities of the proteasome (Supporting Figure S2B). Conversely, bortezomib did not affect ATX activity. We next tested our inhibitors for selectivity against recombinant ENPP1, which is the closest relative of ATX, alkaline phosphatase (AP) and a broad-spectrum phosphodiesterase (PDE). None of these enzymes were affected by the ATX inhibitors at doses up to 10 μM (Supporting Figure S2A). Furthermore, cell viability was not compromised by HA130 (Supporting Figure S2C).

2.5 Inhibition of ATX-driven melanoma cell migration

ATX was originally identified as an autocrine motility factor for human A2058 melanoma cells.[1] We examined the ATX-mediated chemotactic migration of A2058 cells using a Boyden

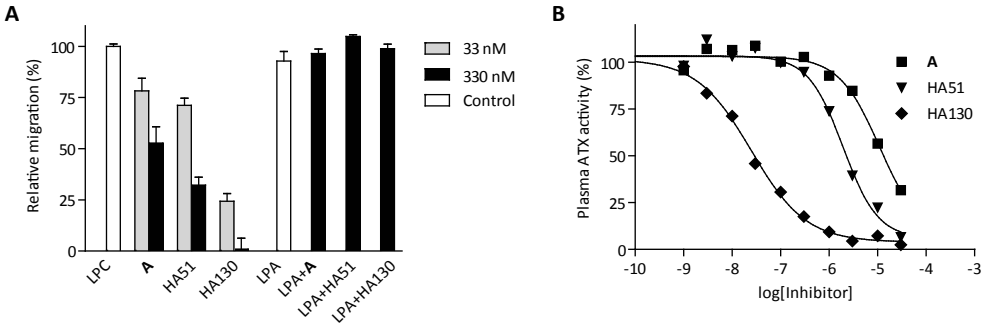

Figure 4: Effect of inhibitors on ATX-induced cell migration and on plasma ATX/lysoPLD activity. (A) ATX (1.2 nM), LPC (1 μM) and BSA (1 mg mL^{-1}) were added to the lower chambers of 48-wells Boyden chambers and the trans-well migration of A2058 melanoma cells was assayed after 4 h in the presence or absence of ATX inhibitors. None of the compounds inhibited LPA-induced cell migration (inhibitor and LPA added at 0.3 μM). (B) Inhibition of endogenous ATX/lysoPLD activity in human plasma *ex vivo*, as measured by choline release from LPC. Inhibition was maintained for at least 24 h (see Supporting Table S1).

chamber assay. ATX hydrolyzes exogenously added LPC into LPA, a potent chemoattractant for A2058 cells. As shown in Figure 4A, ATX inhibitors **A**, HA51 and HA130 inhibited ATX-mediated cell migration with increasing potencies. None of the inhibitors affected LPA-induced cell migration, indicating that they do not act on LPA receptor signaling pathways.

2.6 Inhibition of plasma ATX activity

ATX is identical to plasma lysoPLD[3,4] and responsible for virtually all LPA-producing activity in plasma and serum.[31] Inhibitors were tested for their ability to inhibit ATX/lysoPLD activity in human plasma *ex vivo*. As shown in Figure 4B, all three inhibitors were found to inhibit plasma ATX activity with the expected ranking order of potency. Inhibition of plasma ATX activity was long-lasting (24 h), indicating that HA130 is stable in plasma (Supporting Table S1).

2.7 HA130 decreases circulating LPA levels in mice

To investigate how ATX inhibition affects circulating plasma LPA levels, we administered HA130 (1 nmol g^{-1}) or vehicle as a single bolus injection into the jugular vein of anaesthetized mice. As a non-vehicle control we used compound HA51. Levels of HA130 or LPA in plasma samples rapidly isolated from venous blood were monitored before and after dosing. As shown in Figure 5A, intravenous administration of vehicle or HA51 (Supporting Figure S3) had little or no effect on plasma LPA levels. Following administration of HA130 (t = 10 min), plasma levels of the inhibitor rose rapidly to a concentration approaching 0.35 μM. This was accompanied by a parallel decrease in plasma LPA levels (3.8-fold) which returned slowly towards baseline as plasma levels of HA130 declined. Figure 5B shows summarized data from replicate experiments in which mice

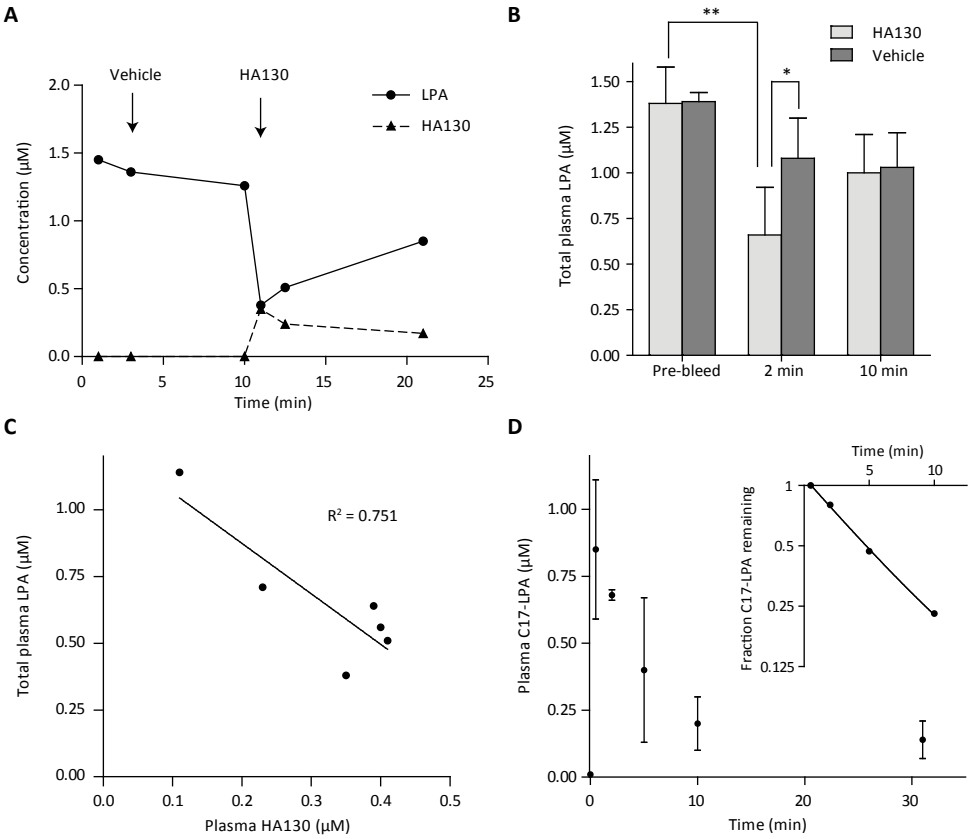

Figure 5: Effects of HA130 on circulating LPA levels in mice. (A) Vehicle or HA130 was administered intravenously into an anaesthetized mouse and plasma levels of the inhibitor or total LPA were determined at the indicated time points. Compound HA51 was used as a non-vehicle control (see Supporting Figure S3). (B) Plasma levels of LPA were determined at baseline and at 2 and 10 min post dosing of vehicle or HA130. The data shown are means +/- SD (6 mice treated with HA130; 5 mice treated with vehicle alone). The difference between baseline LPA levels and LPA levels at 2 min in HA130-treated mice are statistically significant ($p < 0.01$, **) by paired t-test. (C) Plasma levels of LPA and HA130 at 2 min post administration closely correlate ($R^2 = 0.751$). (D) C17-LPA (10 µL of a 10 mM solution in saline containing 0.1% fatty acid-free BSA) was injected into the jugular vein of anaesthetized mice and plasma levels of C17-LPA were determined at different time points. The inset shows a semi-log plot used to calculate the half-life for clearance of C17-LPA from the circulation. Data points are means +/- SD (n = 3).

were dosed with vehicle or HA130 while plasma LPA levels were measured before, 2 and 10 min post dosing (see also Supporting Figure S3). Administration of HA130 produced statistically significant decreases in plasma LPA levels compared to baseline, vehicle and HA51. The mean decrease in plasma LPA levels was 48% of the baseline control at 2 min post administration of HA130. Plasma HA130 levels correlated well ($R^2 = 0.751$) with plasma LPA levels (Figure

5C). Taken together, these findings suggest that continual production of LPA by ATX-catalyzed hydrolysis of circulating LPC is required to sustain plasma levels of LPA at their observed steady-state level. To confirm this, we injected C17-LPA and found that the levels of this unnatural LPA analog were elevated at the earliest measurable time point, but then decayed rapidly following pseudo first-order kinetics with a half-life of approximately 3 min (Figure 5D).

2.8 Discussion and conclusions

In this study we have identified and optimized a class of thiazolidine-2,4-dione compounds as potent and selective inhibitors of ATX that can reduce LPA plasma levels in mice. Our chemical optimization strategy was based on targeting the catalytic T210 residue in ATX by introducing a boronic acid moiety. Boronic acid has previously been shown to be instrumental in the anti-cancer drug bortezomib, which targets the threonine oxygen nucleophile in the active site of the proteasome.[30] Strikingly, replacing the carboxylic acid in HA51 by a boronic acid increased the potency for ATX inhibition by two orders of magnitude compared to the screening hit **A**. This boronic acid inhibitor named HA130 did not affect either ENPP1 or proteasome activity, which have both a catalytic threonine residue. Injection of HA130 into mice resulted in a rapid fall in circulating LPA levels, which is in keeping with the rapid degradation of intravenous administered C17-LPA observed in these animals. This result indicates that maintenance of steady-state LPA levels in plasma involves a highly dynamic balance between its ATX-mediated synthesis and its degradation by LPPs. Consistent with this, LPP1-deficient mice show a significantly reduced rate of [^{32}P]LPA degradation in the bloodstream.[32] Thus, ATX and LPPs are key determinants of LPA turnover *in vivo* and their activity balance sets the steady-state level of LPA in the circulation and, most likely, in the interstitial space.

Several questions concerning circulating ATX remain to be answered, including its tissue origin and metabolic fate, although recent evidence indicates that ATX is rapidly cleared from the circulation by liver sinusoidal endothelial cells.[33] Circulating ATX and LPA do not, of course, reflect the levels in intercellular spaces, since ATX is produced locally by many different cell types while the LPC substrate level in interstitial fluids is much lower than that in plasma. Another key question concerns how ATX activity is regulated under (patho) physiological conditions. Interestingly, ATX binds to activated lymphocytes and platelets in an integrin-dependent manner,[18,21] which could lead to altered catalytic activity and serve as a mechanism for localized LPA production at sites of inflammation and injury.

In conclusion, we have used a boronic acid-based inhibitor to demonstrate that ATX is a valid target for manipulating LPA levels *in vivo*. Further development of boronic acid inhibitors of ATX holds promise for therapeutic use in ATX/LPA-dependent pathologies, including chronic inflammation, tumor progression and fibrotic diseases.

2.9 Experimental section

Chemicals and enzymes. Small molecule libraries were obtained from the NCI and purchased from SPECS (Delft, The Netherlands). The compounds AN-988/40680277, AN-989/41697944 and AN-989/40746701 are all from the SPECS collection and are abbreviated by **A**, **B** and **C**, respectively. 1-Oleoyl-2-hydroxy-*sn*-glycero-3-phosphocholine (LPC, 18:1) and 1-heptadecanoyl-*sn*-glycero-3-phosphate (C17-LPA) were purchased from Avanti Polar Lipids. Horseradish peroxidase (HRP), choline oxidase and phosphodiesterase I from *Crotalus atrox* were obtained from Sigma-Aldrich. Alkaline phosphatase from calf intestine was from Roche. Radiolabeled LPC (1-[1-^{14}C]palmitoyl) was from Amersham Biosciences UK (specific activity 925 kBq mL^{-1}).

Recombinant ATX. HEK293 cells were transfected with the pcDNA3 vector containing a 6xHis-tagged human teratocarcinoma ATX sequence. After transfection, cells were washed and serum-free medium was added and cells were allowed to secrete His-tagged ATX into the culture medium for 48 h. Medium was collected and ATX was purified using TALON-affinity beads (Clontech) as described. Imidazole was removed by dialysis against Tris-buffered saline (140 mM NaCl, 5 mM KCl, 1 mM $CaCl_2$, 1 mM $MgCl_2$ and 50 mM Trizma, pH 8.0). Purity was verified by SDS-PAGE and Coomassie blue staining.

ATX/lysoPLD activity assay.[34] ATX/lysoPLD activity was measured by choline release from LPC (18:1) (40 µM) in 96-well plates. Inhibitors in DMSO were added to recombinant ATX (20 nM) in Tris-HCl buffer (pH 7.4) at 310 K. After 3 h of incubation, 50 µL ABTS (2 mM) and horseradish peroxidase (10 U mL^{-1}) were added to 50 µL of the reaction mixture. Choline oxidase (50 µL, 10 U mL^{-1}) was added for the colorimetric reaction. Absorbance was measured at 405 nm and data were analyzed using Graphpad Prism software. For a more detailed description of this assay see Experimental section Chapter 3.

Phosphodiesterase activity assays.[22] ATX activity toward bis-pNPP hydrolysis was determined as follows. Inhibitors in 2 µL DMSO were added to a 384-wells plate containing 24 µL ATX (~40 nM) in buffer (140 mM NaCl, 5 mM KCl, 1 mM $CaCl_2$, 1 mM $MgCl_2$, 50 mM Tris, pH 7.8) containing fatty acid-free BSA (0.2 mg mL^{-1}). Finally, 24 µL bis-pNPP (2 mM) was added to each well and the plate was incubated for 3 h at room temperature. Percentage inhibition (PI) was determined at a final concentration of 5 µM inhibitor. Absorbance was determined using a Perkin Elmer Envision plate reader (λ = 405 nm). ENPP1 activity was measured at an ENPP1 concentration of 180 nM. Reaction was carried out in 100 µL reaction buffer as described above and incubated at room temperature for 90 min. For PDE activity the same protocol was handed using 6 mU mL^{-1} of PDE incubating the reaction mixture at room temperature for 20 min. Graphpad Prism software was used for data analysis.

^{14}C-LPA formation. Incubations were carried out essentially as described in the choline release assay in the presence of 0.5 µM 1-[1-^{14}C]palmitoyl-LPC. Reactions were terminated by adding 150 µL 0.01 M acetic acid and 250 µL 1-butanol. After mixing and centrifugation, the 1-butanol phase was removed and the remaining water phase extracted with 1-butanol. The pooled butanol phases were washed and concentrated to dryness under vacuum. Reaction products were analyzed by thin layer chromatography (TLC). TLC plates were developed with $CHCl_3$/MeOH/CH_3COOH/H_2O (50:30:8:4). Retardation factors for LPA and LPC were 0.5 and 0.13, respectively. Lipids were visualized by autoradiography.

Selectivity and toxicity. Alkaline phosphatase activity was determined by hydrolysis of bis-*para*-nitrophenyl phosphate (bis-pNPP). Inhibitors were added to 50 µl alkaline phosphate (0.4 U mL^{-1}) in 50 mM Tris-HCl (pH 8.5) containing 0.1 mM EDTA. 50 µL bis-pNPP (0.6 mM) was added to each well and the plate was incubated at room temperature for 1.5 h. Absorbance was determined at a wavelength of 405 nm.

Cell toxicity was determined using the CellTiter-Blue assay. Cells ($1.5x10^5$ mL^{-1}) were incubated with or without inhibitors for 24 h. Phenylarsine oxide (PAO) was used as a control for cell death. After 19 h of incubation, 20 µL of resazurin (0.125 mg mL^{-1}) was added for 5 h. Fluorescence was measured at $\lambda_{ex}/\lambda_{em}$ = 544/560 nm.

Proteasome activity. Purified bovine proteasome was preincubated with inhibitors for 30 min, followed by addition of AMC substrate.[35] Fluorescence was measured every 10 min during 1 hr after substrate addition at 310 K. 1 µg of bovine proteasome was added to assay buffer (25 mM Tris pH 7.4, 5 mM $MgCl_2$, 1 mM DTT, 1 mM ATP). AMC substrates used: 100 µM LLVY-AMC (chymotryptic activity), 40 µM LLE-AMC (caspase-like activity) and 60 µM VGR-AMC (tryptic activity). Controls used for proteasome inhibition were MG132 (25 µM) and epoxomicin (1 µM).

Human plasma ATX activity. Plasma ATX activity was measured in 96-wells plates using LPC (18:1) as a substrate. Heparin-treated human plasma (2 µL) was added to 38 µL Tris-HCl buffer (100 mM Tris-HCl, pH 9, 500 mM NaCl, 5 mM $MgCl_2$ and 0.05% Triton X-100). Subsequently, 0.8 µL inhibitor in DMSO was added. Finally, 40 µL of 2 mM LPC (18:1) in Tris-HCl buffer was added to each well and the plate was incubated at 310 K. The mixture with DMSO alone was used as a control. Plasma without added LPC was taken as control for endogenous LPA production. After 1.5 h of incubation, 150 µL homovanillic acid (2 mM) and horseradish peroxidase (1.6 U mL^{-1}) in Tris-HCl (0.01% Triton X-100, 20 mM $CaCl_2$ and 50 mM Tris-HCl, pH = 7.4) was added to 20 µL of the reaction mixture. Choline oxidase was added (40 µL, 4 U ml^{-1}) and fluorescence was determined at $\lambda_{ex}/\lambda_{em}$ = 320/450nm.

ATX-mediated cell migration. A2058 melanoma cell chemotaxis was assayed using 48-well Boyden chambers. Fibronectin-coated polycarbonate membranes (8 µM pores, NeuroProbe Inc.) were used to separate the upper from the lower chamber. The lower chamber contained DMEM with BSA (1 mg mL^{-1}), ATX (1.2 nM) and LPC (1 µM). Cells (0.75×10^6 mL^{-1}) were loaded in the upper wells and the chamber was incubated at 310 K for 4 h. Non-migrated cells were removed from the membrane and migrated cells were fixed and stained in Diff-Quick (Medion Diagnostics AG, Switzerland). The membrane was mounted on a glass slide and migrated cells were quantified.

Quantitation of HA130 by HPLC tandem mass spectrometry. HA130 was quantitated by HPLC tandem mass spectrometry using an ABI 4000 Q-Trap hybrid linear ion trap triple quadrupole mass spectrometer operating in triple quadrupole mode. The ion source settings were ion spray voltage +5500 V, declustering potential 126 V entrance potential 10 V ion spray voltage 5500 V, ion source temperature 823 K. Material was separated by reverse phase HPLC on an Agilent Eclipse XDB C8 column (4.6 × 150 mm, 5 µM), flow rate 0.5 mL min^{-1} with a step gradient of solvent A 75/25 methanol/water containing 0.5% formic acid and 0.1% ammonium formate, solvent B 99/1 methanol water containing 0.5% formic acid and 0.1% ammonium formate. HA130 was quantitated by selective reaction monitoring of precursor/product ion pairs with m/z 464/109, 464/135.1, 464/117.1 with optimized collision energies and colllision cell exit potentials for each ion pair. For analysis of HA130 in mouse plasma, material was extracted/deproteinated using acidified organic solvents as detailed below. Recovery of HA130 was estimated to be ~70%; values were corrected for recovery of the C17-LPA internal standard (see below).

Quantitation of LPA molecular species by HPLC tandem mass spectrometry. Whole blood was sampled and transferred directly into anticoagulant, centrifuged and plasma added directly to acidified organic solvents. After extraction, organic solvent soluble material was separated by reverse phase HPLC and 16 abundant LPA molecular species quantitated by tandem mass spectrometry using an ABI 4000 Q-Trap hybrid linear ion trap triple quadrupole mass spectrometer. Recovery was determined using C17-LPA as an internal standard and quantitation accomplished by reference to calibration curves determined using a series of synthetic LPAs that were independently quantitated by phosphorous analysis following wet digestion in perchloric acid.

Studies in mice. For intravenous administration, HA130 and HA51 in DMSO were diluted 10-fold into saline to give a drug concentration solution of 1 mM and a final DMSO concentration of 10%. This material was kept at 310 K and bath sonicated for 30 s immediately prior to intravenous administration. Male FVB mice were anaesthetized with isofluorane and dissected to expose the jugular vein. HA130 (1 $\mu L\ g^{-1}$, 1 mM) or vehicle were injected intravenously. HA51 served as a non-vehicle control. Whole blood was sampled from the jugular vein and collected directly into anticoagulant, mixed, centrifuged and plasma transferred to glass tubes containing acidified solvents for extraction of HA130 and LPA. All animal experiments conformed to the recommendations of the "Guide for the Care and Use of Laboratory Animals" (Department of Health, Education, and Welfare publication number NIH 78-23, 1996) and were approved by the institutional Animal Care and Use Committee.

Chemical synthesis inhibitors. See Chapter 3.

2.10 References

1. Stracke, M. L. et al. Identification, purification, and partial sequence analysis of autotaxin, a novel motility-stimulating protein. *J. Biol. Chem.* **267**, 2524-2529 (1992).
2. Stefan, C. Jansen, S. & Bollen, M. NPP-type ectophosphodiesterases: unity in diversity. *Trends Biochem. Sci.* **30**, 542-550 (2005).
3. Tokumura, A. et al. Identification of human plasma lysophospholipase D, a lysophosphatidic acid-producing enzyme, as autotaxin, a multifunctional phosphodiesterase. *J. Biol. Chem.* **277**, 39436-39442 (2002).
4. Umezu-Goto, M. et al. Autotaxin has lysophospholipase D activity leading to tumor cell growth and motility by lysophosphatidic acid production. *J. Cell Biol.* **158**, 227-233 (2002).
5. van Meeteren, L. & Moolenaar, W. Regulation and biological activities of the autotaxin-LPA axis. *Prog. Lipid Res.* **46**, 145-160 (2007).
6. Moolenaar, W. H. van Meeteren, L. A. & Giepmans, B. N. The ins and outs of lysophosphatidic acid signaling. *BioEssays* **26**, 870-881 (2004).
7. Noguchi, K. Herr, D. Mutoh, T. & Chun, J. Lysophosphatidic acid (LPA) and its receptors. *Curr. Opin. Pharmacol.* **9**, 15-23 (2009).
8. Brindley, D. & Pilquil, C. Lipid phosphate phosphatases and signaling. *J. Lipid Res.* **50**, S225-S230 (2009).
9. Sciorra, V. & Morris, A. Roles for lipid phosphate phosphatases in regulation of cellular signaling. *Biochim. Biophys. Acta, Mol. Cell Biol. Lipids* **1582**, 45-51 (2002).
10. Tanaka, M. et al. Autotaxin Stabilizes Blood Vessels and Is Required for Embryonic Vasculature by Producing Lysophosphatidic Acid. *J. Biol. Chem.* **281**, 25822-25830 (2006).

11. van Meeteren, L. A. et al. Autotaxin, a secreted lysophospholipase D, is essential for blood vessel formation during development. *Mol. Cell Biol.* **26**, 5015-5022 (2006).
12. Mills, G. B. & Moolenaar, W. H. The emerging role of lysophosphatidic acid in cancer. *Nat. Rev. Cancer* **3**, 582-591 (2003).
13. Boucharaba, A. et al. Platelet-derived lysophosphatidic acid supports the progression of osteolytic bone metastases in breast cancer. *J. Clin. Invest.* **114**, 1714-1725 (2004).
14. Liu, S. et al. Expression of Autotaxin and Lysophosphatidic Acid Receptors Increases Mammary Tumorigenesis, Invasion, and Metastases. *Cancer Cell* **15**, 539-550 (2009).
15. Nam, S. W. et al. Autotaxin (ATX), a potent tumor motogen, augments invasive and metastatic potential of ras-transformed cells. *Oncogene* **19**, 241-247 (2000).
16. Taghavi, P. et al. In vitro genetic screen identifies a cooperative role for LPA signaling and c-Myc in cell transformation. *Oncogene* **27**, 6806-6816 (2008).
17. Lin, S. et al. The Absence of LPA2 Attenuates Tumor Formation in an Experimental Model of Colitis-Associated Cancer. *Gastroenterology* **136**, 1711-1720 (2009).
18. Kanda, H. et al. Autotaxin, an ectoenzyme that produces lysophosphatidic acid, promotes the entry of lymphocytes into secondary lymphoid organs. *Nat. Immunol.* **9**, 415-423 (2008).
19. Pradère, J. et al. LPA1 Receptor Activation Promotes Renal Interstitial Fibrosis. *J. Am. Soc. Nephrol.* **18**, 3110-3118 (2007).
20. Tager, A. et al. The lysophosphatidic acid receptor LPA1 links pulmonary fibrosis to lung injury by mediating fibroblast recruitment and vascular leak. *Nat. Med.* **14**, 45-54 (2008).
21. Pamuklar, Z. et al. Autotaxin/lysopholipase D and Lysophosphatidic Acid Regulate Murine Hemostasis and Thrombosis. *J. Biol. Chem.* **284**, 7385-7394 (2009).
22. van Meeteren, L. A. et al. Inhibition of autotaxin by lysophosphatidic acid and sphingosine 1-phosphate. *J. Biol. Chem.* **280**, 21155-21161 (2005).
23. Cui, P. McCalmont, W. Tomsig, J. Lynch, K. & Macdonald, T. α- and β-Substituted phosphonate analogs of LPA as autotaxin inhibitors. *Bioorg. Med. Chem.* **16**, 2212-2225 (2008).
24. Ferry, G. et al. S32826, A Nanomolar Inhibitor of Autotaxin: Discovery, Synthesis and Applications as a Pharmacological Tool. *J. Pharmacol. Exp. Ther.* **327**, 809-819 (2008).
25. van Meeteren, L. Brinkmann, V. Saulnier-Blache, J. Lynch, K. & Moolenaar, W. Anticancer activity of FTY720: Phosphorylated FTY720 inhibits autotaxin, a metastasis-enhancing and angiogenic lysophospholipase D. *Cancer Lett.* **266**, 203-208 (2008).
26. Baker, D. et al. Carba Analogs of Cyclic Phosphatidic Acid Are Selective Inhibitors of Autotaxin and Cancer Cell Invasion and Metastasis. *J. Biol. Chem.* **281**, 22786-22793 (2006).
27. Parrill, A. et al. Virtual screening approaches for the identification of non-lipid autotaxin inhibitors. *Bioorg. Med. Chem.* **16**, 1784-1795 (2008).
28. Adams, J. et al. Potent and selective inhibitors of the proteasome: Dipeptidyl boronic acids. *Bioorg. Med. Chem. Lett.* **8**, 333-338 (1998).
29. Kropff, M. et al. Bortezomib in combination with intermediate-dose dexamethasone and continuous low-dose oral cyclophosphamide for relapsed multiple myeloma. *Br. J. Haematol.* **138**, 330-337 (2007).
30. Groll, M. Berkers, C. Ploegh, H. & Ovaa, H. Crystal Structure of the Boronic Acid-Based Proteasome Inhibitor Bortezomib in Complex with the Yeast 20S Proteasome. *Structure* **14**, 451-456 (2006).

31. Nakasaki, T. et al. Involvement of the Lysophosphatidic Acid-Generating Enzyme Autotaxin in Lymphocyte-Endothelial Cell Interactions. *Am. J. Pathol.* **173**, 1566-1576 (2008).
32. Tomsig, J. L. et al. Lipid phosphate phosphohydrolase type 1 (LPP1) degrades extracellular lysophosphatidic acid in vivo. *Biochem. J.* **419**, 611-618 (2009).
33. Jansen, S. et al. Rapid clearance of the circulating metastatic factor autotaxin by the scavenger receptors of liver sinusoidal endothelial cells. *Cancer Lett.* **284**, 216-221 (2009).
34. Cui, P. et al. Synthesis and biological evaluation of phosphonate derivatives as autotaxin (ATX) inhibitors. *Bioorg. Med. Chem. Lett.* **17**, 1634-1640 (2007).
35. Elliott, P. J. Soucy, T. A. Pien, C. S. Adams, J. & Lightcap, E. S. Assays for proteasome inhibition. *Methods Mol. Med.* **85**, 163-172 (2003).

2.11 Supporting information

Supporting Table S1: Inhibition of ATX activity in human plasma over time.

	PI (%) [a]			
	2h	**4h**	**8h**	**24h**
A	23	26	20	20
HA51	79	83	78	73
HA130	94	100	100	95

[a] Percentage inhibition (PI) by the three inhibitors (5 µM) was measured at the indicated time points. ATX inhibition was constant over 24 h.

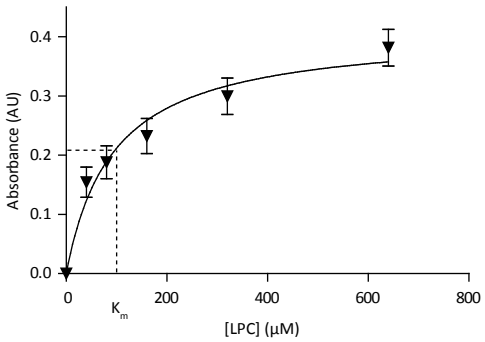

Supporting Figure S1: Saturation kinetics of ATX. Rates of choline release from LPC are plotted against increasing concentration of LPC. ATX activity data points (absorbance; arbitrary units (AU)) were fitted to the Michaelis-Menten equation, yielding an apparent K_m value for LPC of 95 µM (n=5).

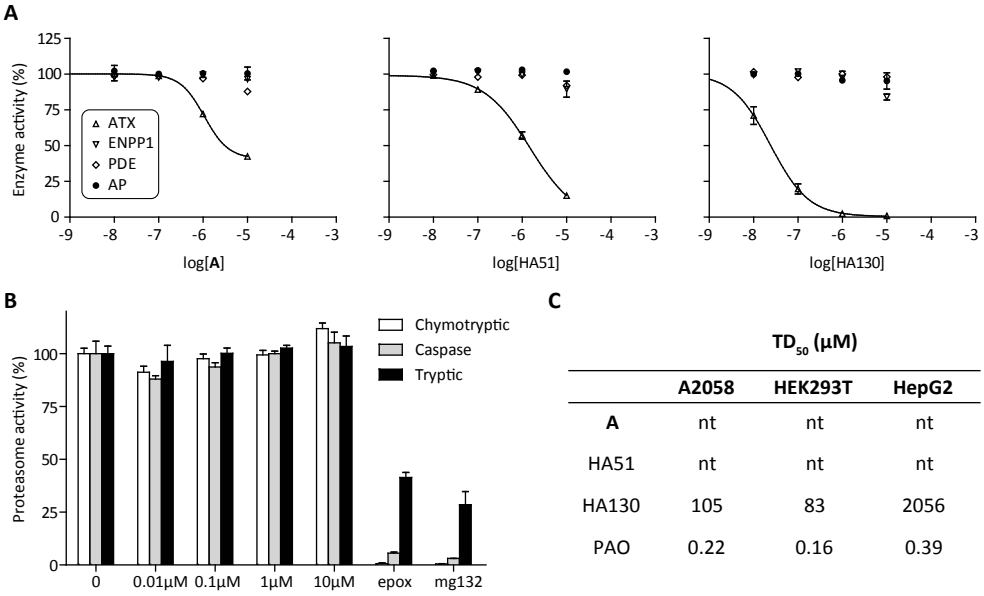

C

	TD_{50} (µM)		
	A2058	**HEK293T**	**HepG2**
A	nt	nt	nt
HA51	nt	nt	nt
HA130	105	83	2056
PAO	0.22	0.16	0.39

Supporting Figure S2: Enzyme selectivity and toxicity of ATX inhibitors. (A) Lack of effect of ATX inhibitors on ENPP1, PDE and AP activity. (B) Lack of effect of HA130 (up to 10 µM) on the indicated proteasome activities. Proteasome inhibitors epoxomicin (epox) and MG132 were used as controls. (C) Toxic dose (TD_{50}) of ATX inhibitors for human A2058, HEK293T and HepG2 cells. Phenylarsine oxide (PAO) was used as a control for cell death (nt: no toxicity below 100 µM).

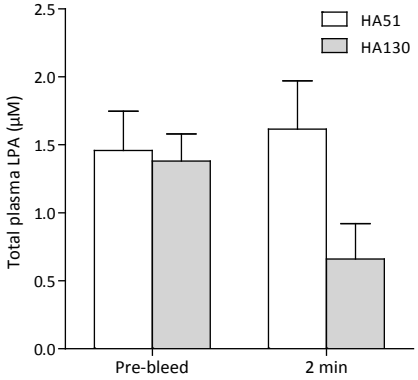

Supporting Figure S3: Plasma levels of LPA were determined before and 2 min post dosing of mice treated with HA51 (n=4) and HA130 (n=6). The data shown are means +/- SEM.